An LCC-Based String-to-Cell Battery Equalizer With Simplified Constant Current Control

Zhengqi Wei, *Graduate Student Member, IEEE*, Faxiang Peng, and Haoyu Wang, *Senior Member, IEEE*

***Abstract*—Constant current equalization can effectively mitigate the inconsistency of battery strings in a fast manner. In this manuscript, a constant current string-to-cell battery equalizer with an open-loop current control is proposed. The equalization scheme is based on LCC multiresonant topology. It utilizes a common equalizer unit shared by each unbalanced cell to transfer energy from the entire string to a single cell. A constant balancing current is achieved with simple fixed-frequency open-loop control. The equalization speed is determined by the predesigned balancing current. Design considerations of the proposed equalizer are analyzed in detail, which ensure zero-voltage switching among all MOSFETs during the equalization process. An experimental platform to balance four lithium-ion battery cells is designed to verify the system performance. Experimental results validate the functionality and analysis of this equalizer. Compared with the conventional architecture, the proposed architecture exhibits a high efficiency, low components count, and obviously reduced control complexity.**

***Index Terms*—Battery equalizers, battery management system (BMS), electric vehicles (EVs), LCC converter, zero-voltage switching (ZVS).**

I. Introduction

LITHIUM-ION batteries are widely utilized in energy storage systems due to their high energy density, low self-discharge rate, and no memory effect [1]. Since the terminal voltage of lithium-ion cell is low, in high-power applications, a large number of battery cells are usually connected in series [2]. However, the differences in battery capacity and internal resistance lead to the mismatch among the batteries connected in series. Fig. 1 illustrates the natural state-of-charge (SOC) distribution of 95 unbalanced series batteries from an electric bus with a mileage of 32 500 km [3], [4]. As indicated in Fig. 1, mismatch might incur some issues such as follows.

1) *Undercharging:* A number of cells within the string is left below its maximum capacity when charging is finished. This limits the overall capacity of the battery pack [5].

2) *Overcharging:* Red bar shows a cell charging touched safety threshold which may result in overcharging and overheating of the battery. This leads to a reaction of the active components with electrolyte and with each other ultimately, inducing explosion and fire [6].

3) *Underdischarging:* When the voltage of a battery (yellow bar) in cell string reaches its lower safety threshold, there are still batteries not completely discharged. This results in a reduction in the usable energy of the batteries [7].

4) *Overdischarging:* Yellow bars indicate if the lower safety threshold is touched, the cell can further be overdischarged, which might incur depletion-induced hazards. In this state, the battery exhibits thermal instability, permanent capacity loss, and possible short circuit [8].

To resolve these issues, battery equalizers are required to mitigate these mismatches. In general, fast equalization speed and simplified control are desired features of battery equalization systems.

Balancing schemes are divided into passive and active methods. Passive methods (cell-to-resistor, C2R) transduce excess energy from cells into heat with shunting resistors [9]. The energy dissipation leads to zero efficiency and heat management problems. Active methods are mainly divided into four balancing categories: cell-to-cell (C2C) [10]–[14], cell-to-string (C2S) [15]–[17], hierarchical module equalizer (HME) [18]–[21], and string-to-cell (S2C) [22]–[26].

C2C method transfers energy from a higher voltage cell to a lower voltage cell. However, its equalization speed is usually slow because of the trivial voltage gap [27]. C2S method [17] presents a flexible energy flow. However, in this structure, each cell requires a separate transformer winding. This leads to bulky magnetics when the number of cells scales up. As discussed in [18], HME method employs a multiwinding transformer to achieve energy transfer among cell packs. This structure is featured with low switch count. However, HME requires multilevel equalizers to balance single cells in submodule, which increases the control complexity.

Balancing speed is a crucial parameter to evaluate the performance of the battery equalizer. Indeed, it is mainly determined by the balancing current. In [6] and [28], different active equalization structures are compared. Among them, S2C structure

Manuscript received May 11, 2021; revised July 2, 2021; accepted July 28, 2021. Date of publication August 5, 2021; date of current version October 15, 2021. This work was supported in part by the National Natural Science Foundation of China under Grant 52077140 and in part by Shanghai Rising Star Program under Grant 20QA1406700. Recommended for publication by Associate Editor A. Gupta. *(Corresponding author: Haoyu Wang.)*

Zhengqi Wei and Haoyu Wang are with the Power Electronics and Renewable Energies Laboratory, School of Information Science and Technology, ShanghaiTech University, Shanghai 201210, China (e-mail: weizhq1@shanghaitech.edu.cn; wanghy@shanghaitech.edu.cn).

Faxiang Peng is with the Faxiang Peng is with the Power Electronics and Renewable Energies Laboratory, School of Information Science and Technology, ShanghaiTech University, Shanghai 201210, China, and also with the Intel Asia-Pacific Research & Development Ltd., Shanghai 200241, China (e-mail: pengfx@shanghaitech.edu.cn).

Color versions of one or more figures in this article are available at https://doi.org/10.1109/TPEL.2021.3102627.

Digital Object Identifier 10.1109/TPEL.2021.3102627

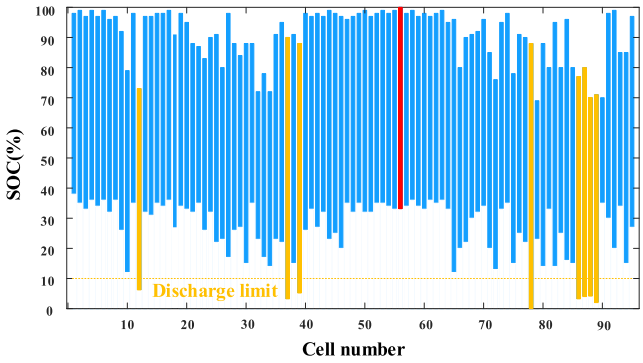

Fig. 1. Natural state-of-charge (SOC) distribution of 95 unbalanced series batteries [3], [4].

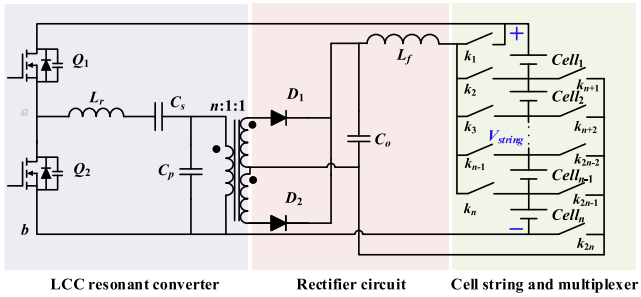

Fig. 2. Schematic of the proposed LCC-based S2C equalizer.

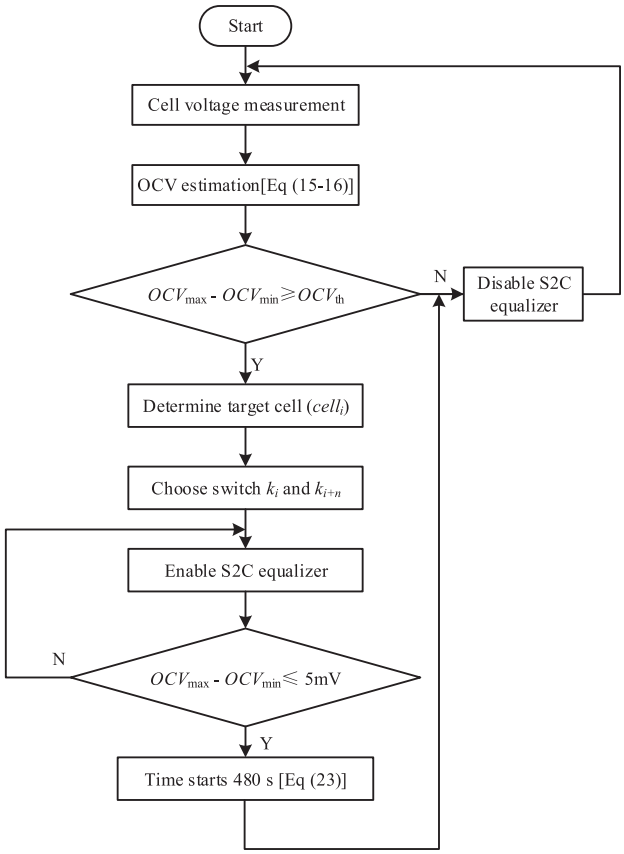

Fig. 3. Flowchart of the proposed S2C equalization algorithm.

can obtain large balancing current because of large voltage differences between the string and unbalanced cells. Thus, these structures are suitable in scenarios with the voltage of single cell lower than the average voltage.

In [22]–[26], S2C structures are investigated to balance the cell voltages. S2C equalizers are typically employed in scenarios with certain cells undercharged. A flyback converter is adopted as the equalization unit. Its size is usually large due to the bulky multiwinding transformer. Generally, constant current S2C equalizers require closed-loop control with dedicated current sensors, which increases components count and control complexity.

In order to achieve high balancing speed and simple control, a fixed-frequency control S2C equalizer is proposed based on LCC converter. The attractive features include the following.

1) It is able to achieve the charge transfer from the string to a single cell. In addition, the high-voltage battery cell can transfer its charge to the low-voltage battery cell via the battery string. This minimizes the number of balancing cycles.

2) The proposed equalizer has good constant current-balancing characteristics. The current can be customized by properly designing the circuit parameters.

3) Due to the output characteristic of LCC resonant converter, only a pair of complementary driving signals with fixed switching frequency is required. This simplifies the circuit design and reduces the control complexity.

4) Both MOSFETs can realize zero-voltage switching (ZVS) turn-ON, and both diodes can realize ZCS turn-OFF. This reduces the switching loss and enables a high switching frequency.

5) The proposed equalization structure can be easily configured in the hierarchical structure. This improves the circuit's extensibility.

The rest of this article is organized as follows. In Section II, the operation principles are detailed performed and the equalization current is analyzed. In Section III, a comprehensive design methodology is presented and the recovery-effect immune equalization strategy is shown which introduced to improve the balancing accuracy. The functionality of the balancing circuits is validated experimentally in Section IV. A comprehensive comparison is given in Section V. Finally, Section VI concludes this article.

II. Operation Principles

A. Proposed Equalizer

The schematic of the proposed equalizer is plotted in Fig. 2. As shown, it is based on a shared LCC resonant converter. Different energy flow paths from the string to cell/substring can be directly established by properly configuring the multiplexer network ($k_1 - k_{2n}$) [29]. Therefore, the multiplexer facilitates both shared transformer and the hierarchical structure which reduces components count. The filter inductor placed behind the capacitor can help improve the constant current performance. The control method for the S2C equalizer is shown in the flowchart in Fig. 3. However, the recovery effect need to be considered in equalization process, and detailed analysis for the compensation operation is performed in Section III.

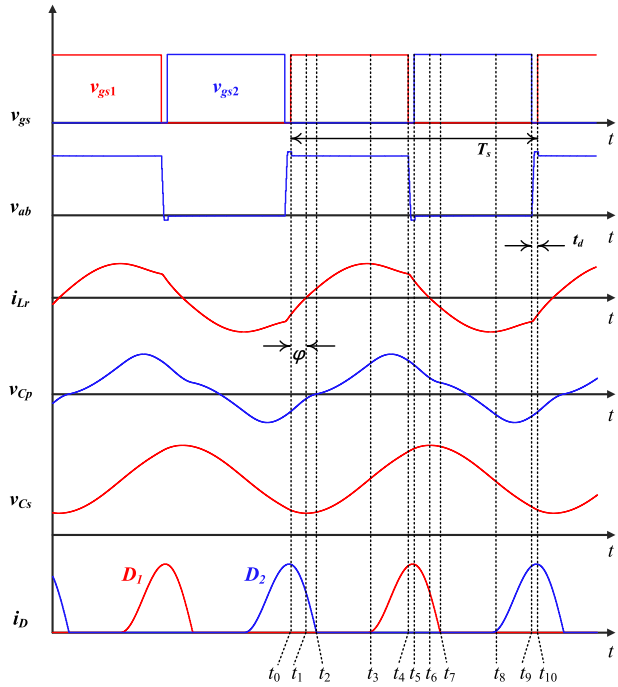

Fig. 4. Key steady-state waveforms.

B. Operation Principles

Fig. 4 demonstrates the key waveforms of the LCC-based equalizer. The equalizer only requires two complementary pulse width modulation (PWM) signals with 50% duty cycle to drive the MOSFETs. The operation of the equalization unit can be divided into ten modes. Their equivalent circuits of four batteries are illustrated in Fig. 5, where Cell_4 is selected as target-balancing cell. Each mode can be described briefly as follows.

Mode 1: As shown in Fig. 5(a), at $t = t_0$, Q_1 is turned ON with ZVS, and Q_2 remains OFF. At this instant, i_{Lr} returns to zero, and the current direction on the leakage inductor is to the left. The resonant tank discharges the battery string through Q_1.

Mode 2: As shown in Fig. 5(b), at $t = t_1$, i_{Lr} increases from zero. Meanwhile, the terminal voltage of C_p (v_{Cp}) decreases to zero.

Mode 3: As shown in Fig. 5(c), at $t = t_2$, the parallel resonant capacitor C_p begins to be charged, and leakage inductance does not participate in resonance. Thus, two rectification diodes on the secondary of the transformer are reversely biased.

Mode 4: As shown in Fig. 5(d), at $t = t_3$, i_{Lr} decreases. The current on the leakage inductor is directed to the right. The rectifier diode (D_1) begins to conduct.

Mode 5: As shown in Fig. 5(e), at $t = t_4$, Q_1 is turned OFF, C_{oss1} starts to be charged, while C_{oss2} starts to be discharged. During the dead band, i_{Lr} commutes to Q_2 and flows through its body diode. This means that the body diode conducts before Q_2 turns ON. This creates the ZVS condition for Q_2.

Starting at t_5, the resonant converter starts to work in the other half cycle, which is similar to the first half cycle.

C. Balancing Current

First harmonics analysis (FHA) method is used to analyze the circuit [30]. The current gain of LCC converter is expressed as

$$G_I = \frac{1}{\sqrt{Q_r^2(1+C_n)(1-f_n^2)+j(f_n-\frac{1}{f_n}\frac{C_n}{1+C_n})^2}} \quad (1)$$

where C_n is the capacitance ratio ($C_n = C_p/C_s$), f_n is the normalized frequency ($f_n = f_s/f_0$), f_0 is the resonant frequency, and Q_r is the quality factor of the resonant tank ($8n^2V_{Cell}/(\pi^2 I_o Z_r)$).

The curves of current gain versus normalized frequency under different load conditions are depicted in Fig. 6. As shown, the curves converge at $f_n = 1$. This means the LCC-based equalizer should be designed to operate at the resonant frequency. Therefore, the balancing current is determined by the input voltage and resonant tank parameters while it is independent of load.

III. Key Design Considerations

A. Design Methodology of the Proposed S2C Equalizer

Fig. 7 illustrates the design method of proposed equalizer. To design such a S2C and overall optimized equalization structure, the following considerations should be included.

1) To obtain constant balancing current, the resonant tank parameters need to be properly designed.

2) To achieve a high conversion efficiency, the significant switching loss in high switching frequency is reduced by addressing the optimal design considerations of LCC, which ensures ZVS turn-ON of all MOSFETs.

3) To improve balancing accuracy, target cell should be equalized according to the open-circuit voltage (OCV). In addition, the recovery effect of battery needs to be compensated.

B. Resonant Tank Parameters

According to the analysis, the resonant tank parameters are the key parameters which determine the circuit performance. Gilbert *et al.* [31] proposed the design methodology of LCC converter as constant current source. To optimize and simplify the design, the following considerations should be addressed.

1) Capacitance ratio (C_n): As shown in Fig. 8, when $\omega_n = 1$, current gain increases rapidly with the increase of C_n. When C_n is high, the current gain curves become steep. This leads to sharp change of balancing current with slight change of f_s. When C_n is low, low current gain leads to high resonant tank current, which degrades the efficiency. Therefore, the range of C_n is selected between 0.1 and 0.2.

2) Turns-ratio (n): The equalizer operates in constant current mode, and resonant tank current increases when turns-ratio is low. This leads to high power loss. High turns-ratio requires bulky transformer.

3) Resonant tank parameters: Fig. 9 shows the equivalent circuit when Cell_4 is underbalanced. The cells are modeled by an ideal voltage source with certain internal resistance. More detailed battery model will be analyzed below. The current gain

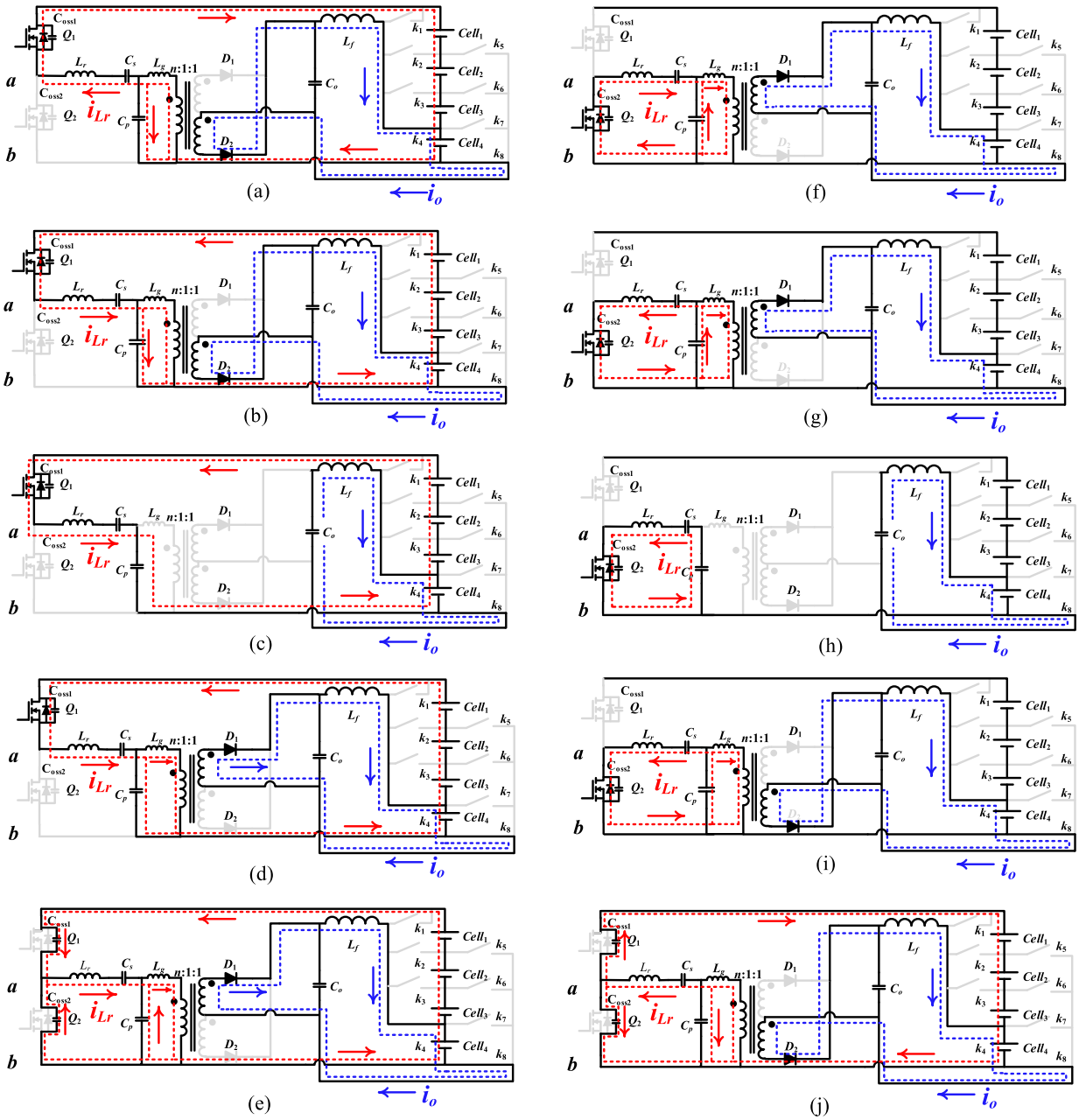

Fig. 5. Equivalent circuit of the equalizer to balance four batteries. (a) Mode 1 ($t_0 - t_1$]. (b) Mode 2 ($t_1 - t_2$]. (c) Mode 3 ($t_2 - t_3$]. (d) Mode 4 ($t_3 - t_4$]. (e) Mode 5 ($t_4 - t_5$]. (f) Mode 6 ($t_5 - t_6$]. (g) Mode 7 ($t_6 - t_7$]. (h) Mode 8 ($t_7 - t_8$]. (i) Mode 9 ($t_8 - t_9$]. (j) Mode 10 ($t_9 - t_{10}$].

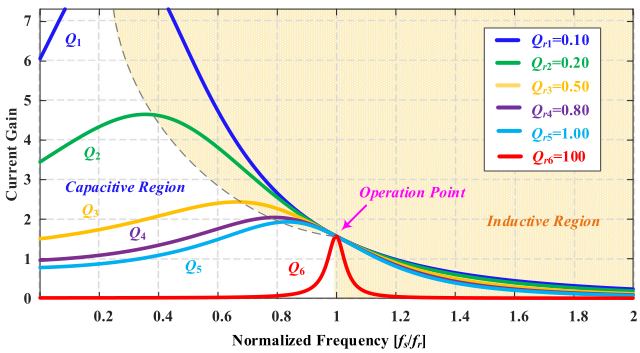

Fig. 6. Current gain curves versus normalized f_n.

G_I can be derived as

$$G_I = \frac{Z_p // R_{eq}}{Z_{rs} + Z_p // R_{eq}} \cdot \frac{1}{R_{eq}}. \tag{2}$$

The impedance of each element of the resonant tank can be expressed as

$$\begin{cases} Z_{rs} = j\omega_s L_r + \dfrac{1}{j\omega_s C_s} \\ Z_p = \dfrac{1}{j\omega_s C_p}. \end{cases} \tag{3}$$

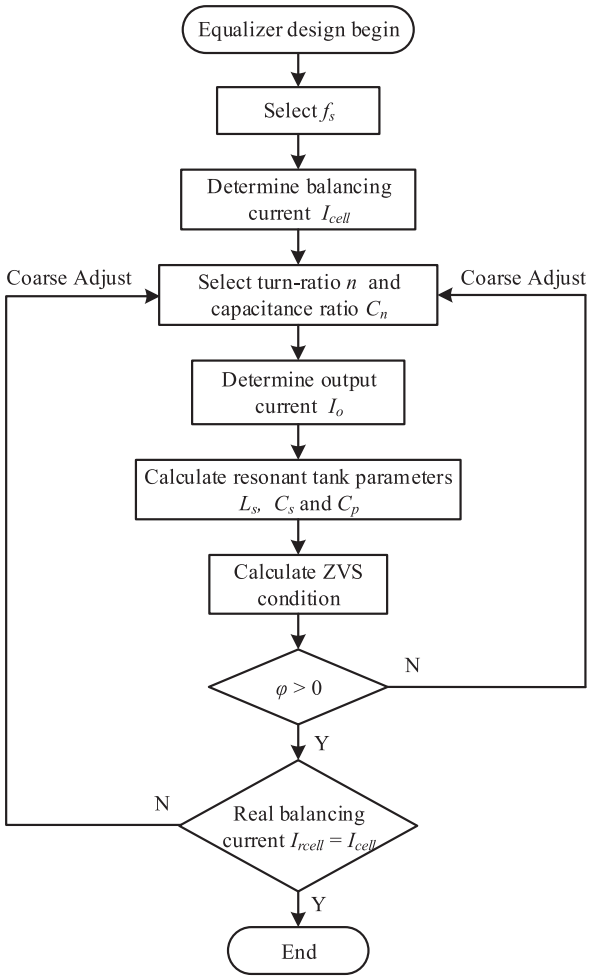

Fig. 7. Design flowchart of the proposed S2C equalizer.

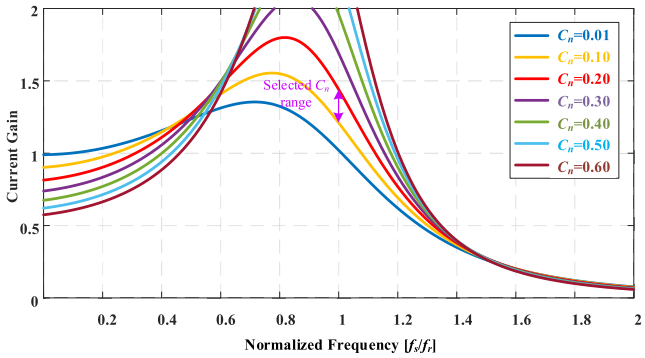

Fig. 8. Current gain versus normalized frequency with different capacitance ratios.

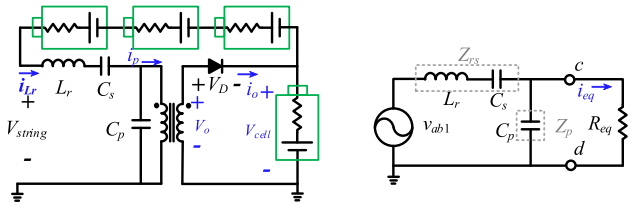

Fig. 9. Equivalent circuit when Cell_4 is underbalanced.

Resonant angular frequency of LCC converter can be derived as

$$\omega_0 = \sqrt{\frac{C_s + C_p}{L_r C_s C_p}}. \tag{4}$$

When the switching frequency is equal to the resonant frequency ($\omega_s = \omega_0$), the modulus of current gain can be derived as

$$|G_I| = C_n \sqrt{\frac{C_s}{L_r}\left(\frac{1}{C_n} + 1\right)}. \tag{5}$$

The fundamental component of v_{ab} (v_{ab1}) is expressed as

$$v_{ab1} = \frac{2V_{\text{string}}}{\pi} \sin(\omega_s t). \tag{6}$$

The output current i_{eq1} is expressed as

$$i_{eq1} = \frac{\pi I_o}{2n} \sin(\omega_s t + \theta). \tag{7}$$

Combing equations (2)– (7), the resonant tank parameters can be derived as

$$\begin{cases} L_r = \dfrac{2nV_{\text{string}}(1 + C_n)}{\pi^3 f_s I_o} \\ C_s = \dfrac{\pi I_o}{8nV_{\text{string}} C_n f_s} \\ C_p = \dfrac{\pi I_o}{8nV_{\text{string}} f_s}. \end{cases} \tag{8}$$

C. ZVS Conditions

To minimize the switching loss, it is preferable that all MOSFETs are turned ON with ZVS. To realize ZVS of a MOSFET, the body diode should conduct before the MOSFET does.

The equivalent impedance across ab can be derived as

$$\begin{aligned} Z_n &= j\omega_s L_r + \frac{1}{j\omega_s C_s} + \frac{1}{j\omega_s C_p} // R_{eq} \\ &= \frac{R_{eq}}{C_p^2 R_{eq}^2 \omega_s^2 + 1} + j\left(L_r \omega_s - \frac{1}{C_s \omega_s} - \frac{C_p R_{eq}^2 \omega_s}{C_p^2 R_{eq}^2 \omega_s^2 + 1}\right). \end{aligned} \tag{9}$$

The resonant current can be expressed as

$$i_{Lr} = \frac{v_{ab1}}{Z_n} = \frac{2V_{\text{string}}}{\pi |Z_n|} \sin(\omega_s t + \varphi). \tag{10}$$

According to (10), when LCC resonant converter operates at resonant frequency ($\omega_n = 1$), the impedance angle can be derived as

$$\varphi = \arctan\left(\frac{1}{R_{eq}(1 + C_n)} \sqrt{\frac{L_r(1 + C_n)}{C_p}}\right). \tag{11}$$

The phase of output voltage leads the phase of output current ($\varphi > 0$), which is the necessary condition to realize ZVS. In addition, the dead time t_d must be properly designed to ensure both ZVS turn-ON of S1 and a minimized circulating current. This means

$$\int_0^{t_d} -\frac{2V_{\text{string}}}{\pi |Z_n|} \sin(\omega_s t + \varphi)\, dt \geqslant 2C_{\text{oss}} V_{\text{string}}. \tag{12}$$

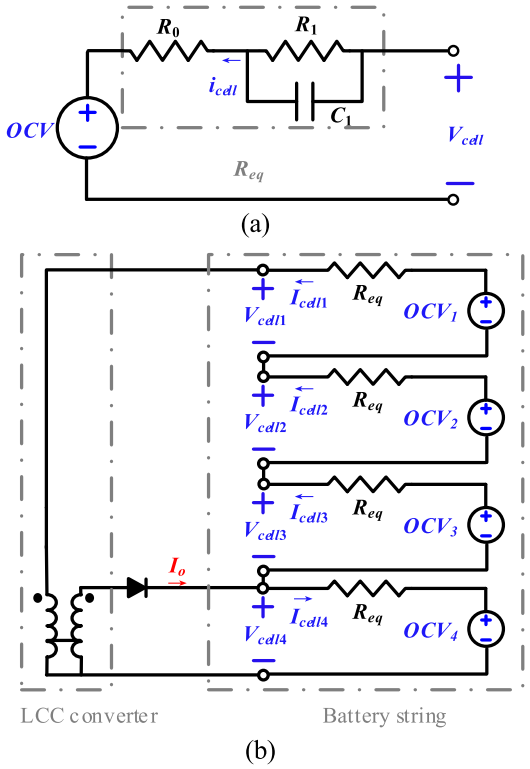

Fig. 10. Equivalent circuit model of the lithium-ion battery. (a) Simplified Thevenin battery model. (b) Equivalent circuit of the basic equalizer unit with four cells.

Thus, the dead band should be designed as

$$\frac{1}{\omega_s}\{\arccos[\pi\omega_s C_{\text{oss}}|Z_n| + \cos(\varphi)] - \varphi\} \leqslant t_d \leqslant \frac{\varphi}{2\pi}T_s. \tag{13}$$

D. Open-Circuit Voltage Estimation

OCV is monotonously related to the battery SOC. Due to the existence of internal resistance, the OCV is not equal to the measured terminal voltage (V_{cell}). Therefore, equalization judgment may not be accurate. In order to improve the equalization accuracy, the Thévenin-based electrical model [32] is used in the Li-ion battery model [33]. Its simplified schematic is illustrated in Fig. 10(a), where the dc voltage source represents OCV, V_{cell} is the terminal voltage, R_0 is the ohmic resistance, R_1 is dynamic resistance, C_1 is the corresponding dynamic capacitance, and i_{cell} is the terminal current.

The equivalent circuit diagram of the proposed voltage equalizer with four cells is shown in Fig. 10(b); the basic LCC resonant converter can be modeled as a dc transformer, cell string (Cell_1 - Cell_4) is source, and single cell (Cell_4) is the target. Thus, OCV is estimated by

$$i_{\text{cell1}} = i_{\text{cell2}} = i_{\text{cell3}} = i_{\text{cell}} \tag{14}$$

$$\text{OCV}_{1,2,3} = V_{\text{cell1,2,3}} - i_{\text{cell}}R_{eq} \tag{15}$$

$$\text{OCV}_4 = V_{\text{cell4}} + i_{\text{cell4}}R_{eq}. \tag{16}$$

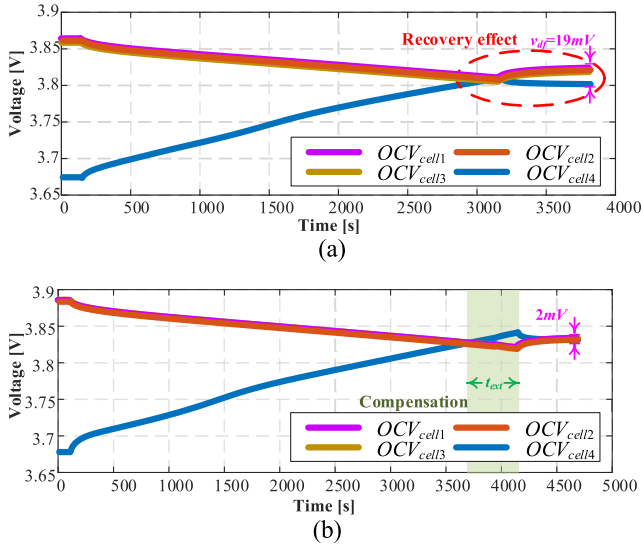

Fig. 11. Open-circuit voltages with different equalization stages. (a) Without recovery effect compensation. (b) With recovery effect compensation.

The relationship between i_{cell3} and i_{cell4} is expressed as

$$i_o = i_{\text{cell3}} + i_{\text{cell4}}. \tag{17}$$

The equivalent internal resistance (R_{eq}) can be measured experimentally by the pulse-current discharge method [27]. The voltage drop across the battery internal resistance affects the accuracy of balancing judgment. Compensating the impact of R_{eq} can improve the accuracy of equalization.

E. Recovery Effect Compensation

Generally, due to the battery recovery effect, the OCV becomes stable only after a certain idle time. This phenomena is caused by slow diffusion processes in the cell, so this slowly changing voltage is called diffusion voltage. Then, the OCV can accurately characterize SOC [34]. However, in practical equalization process, this effect affects the judgment of the end of balancing. The recovery effect can be clearly observed in the experimental results as shown in Fig. 11(a). In order to improve the accuracy of equalization, battery recovery should be considered in the process of equalization. The diffusion voltage of the battery falls after the charging and rises after discharging. The diffusion voltage (v_{df}) can be expressed as

$$v_{df} = R_1 i_{\text{cell3}} + R_1 i_{\text{cell4}} = R_1 i_o. \tag{18}$$

Thus, the charge need to be transferred in extended time is

$$Q_{\text{ext}} = \eta \cdot (i_{\text{cell3}} + i_{\text{cell4}}) \cdot t_{\text{ext}} = \eta i_o t_{\text{ext}} \tag{19}$$

where η is balancing efficiency. According to [35], the slope of OCV versus SOC curve is expressed as

$$k_{\text{SOC}} = \frac{\Delta v}{\Delta \text{SOC}}. \tag{20}$$

The slope of the OCV versus time curve of the target cell and source cell is expressed as

$$k_t = \frac{\Delta v}{\Delta t} = \eta i_{\text{cell4}} k_{\text{SOC}} \tag{21}$$

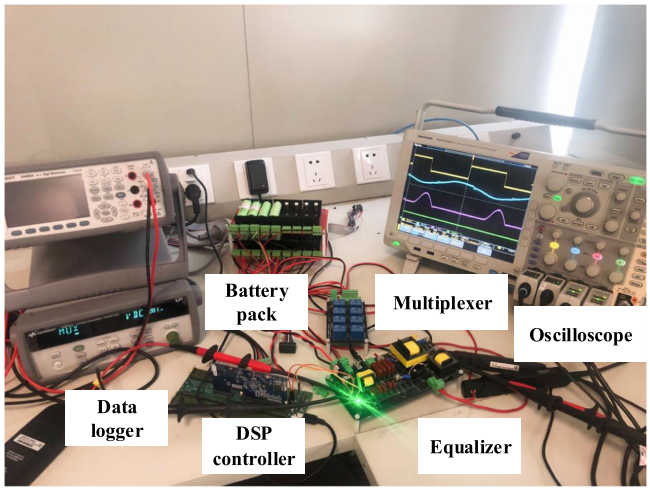

Fig. 12. Photograph of experimental setup.

$$k_s = \frac{\Delta v}{\Delta t} = -\eta i_{\text{cell3}} k_{\text{SOC}}. \tag{22}$$

The change of OCV in the compensation process should be equal to the diffusion voltage. Therefore, combining (18)–(22), the extended time is estimated as

$$t_{\text{ext}} = \frac{R_1}{\eta k_{\text{SOC}}}. \tag{23}$$

Therefore, the equalization process needs to be extended to compensate for the voltage change after the equalization stops [21]. As shown in Fig. 11(b), when extended balancing time is enforced, the OCV converges eventually due to the battery recovery effect. Using this method, a more accurate balancing can be achieved. Since the model is simplified, we adjust the time with the experimental results.

IV. Experimental Verification

In order to validate the analysis of the proposed equalizer, an experimental prototype to balance four series-connected lithium-ion cells (2900 mAh) is implemented. Fig. 12 showcases the test bench. The circuit parameters are listed in Table I. NCR18650PF lithium-ion cells are employed in the prototype. The module multiplex network is implemented by relays (SRD05VDC).

Fig. 13(a) shows the key waveforms of Q_1 and v_{Cs}. Fig. 13(b) shows the waveforms of v_{gs2}, capacitor voltage v_{Cp}, diode current i_{D2}, and output current i_o. As shown, both Q_1 and Q_2 are turned ON with ZVS, which verifies the theoretical analysis.

As shown in Fig. 14, when the proposed equalizer output voltage is equal to the change of load in the real process of single cell battery balancing, the output balancing current is approximately 505 mA. When the load range is equal to three batteries, the output current variation is less than 5%. It indicates that the proposed equalizer exhibits a good open-loop constant current behavior. In addition, the peak efficiency of 88.1% is achieved when the output power is 2.67 W.

Fig. 15 shows the experimental terminal voltage and open-circuit voltage of every single cell during two different working scenarios. The voltage data is recorded by a data logger (Keysight 34972 A). In Fig. 15(a) and (b), three cells have identical initial voltages (3.882 V), while the target cell has its initial voltage lower than the average voltage. This setting emulates the scenario when a cell has its voltage obviously lower than the average voltage of the string. As demonstrated, when the balancing stops, a recovery phenomenon of each cell is observed. Therefore, the balancing time needs to be extended to ensure

TABLE I
Design Parameters of the Equalizer

Component Type	Parameters
Microcontroller	TMS320F28379
MOSFET	BSC052N03LS
MOSFET driver	ACPL-W343
Relay	SRD-05VDC
Relay driver	TDB62083AFWG
Diode	STPS5L60S
Battery	NCR18650PF
Monitor IC	BQ76PL536
Switching frequency(f_s)	200 kHz
Transformer (EI40) turns ratio(n)	14:7:7
Resonant inductor (L_r)	18.4 μH
Series capacitor (C_s)	236.8 nF
Parallel capacitor (C_p)	40.3 nF

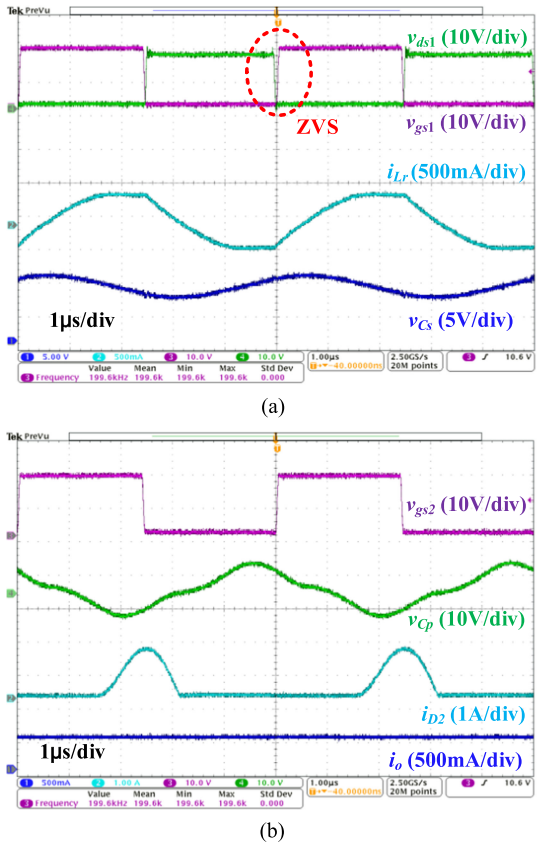

Fig. 13. (a) v_{gs1}, v_{ds1} of Q_1, series capacitor voltage v_{Cs}, and inductor current i_{Lr}. (b) v_{gs2}, parallel capacitor voltage v_{Cp}, diode current i_{D3} and i_o.

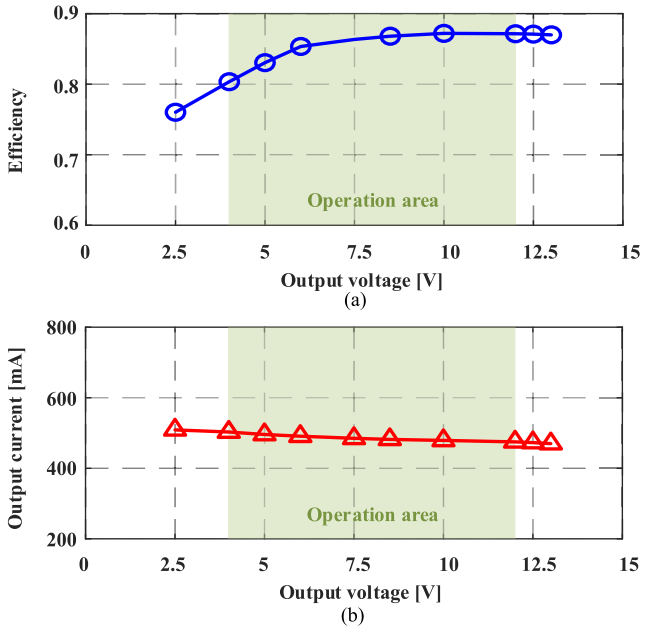

Fig. 14. Experimentally measured (a) conversion efficiency and (b) output current of the LCC-based equalizer versus output voltage.

that the voltages converge. The experimental results show that when the voltage of a certain battery is lower than the threshold voltage, the equalization circuit reduces the voltage difference from 204 to 3 mV in 4100 s. Fig. 15(c) shows the equalization result for four cells whose initial voltages are about 3.880, 3.880, 3.683, and 3.682 V, respectively. The energy flow is from the cell string (four cells) to the cell substring (two cells). As indicated, the equalizer reduces the voltage difference from 198 to 3 mV in 4000 s. Fig. 15(d) shows the equalization result for four cells whose initial voltages are about 3.839, 3.841, 3.839, and 3.673 V, respectively. When the open-circuit voltage difference is lower than 5 mV, the balancing process lasts 480 s. The OCV difference is reduced to 5 mV.

In order to further validate the proposed concept, Fig. 16(a) and (b) shows the equalization results for four cells with different distributions. At first, the entire battery pack transfers energy to the lowest voltage battery (Cell_1). Then, when the voltage of Cell_1 is higher than Cell_2, the pack balances the energy to Cell_1 and Cell_2 simultaneously. Finally, the battery pack transfers charge to substring (Cell_1, Cell_2, and Cell_3). It can be observed that under any cell combination, the proposed system can balance the target cell voltages in turn toward the average value. The equalization circuit reduces the voltage difference from 223 to 14 mV in 5300 s, and the equalizer reduces the voltage difference from 192 to 16 mV in 4900 s.

In Fig. 17, balancing experiments are conducted with 400 mA charge/discharge current. When the OCV of a battery is lower than the threshold, the power of the entire battery string will be limited during the charging process. Thus, in charging test [Fig. 17(a)], the initial voltages (OCV) are set to 3.828, 3.827, and 3.824 V for strong cells, and 3.701 V for the weak cell. After 2600 s, the voltage difference decreases from 127 to 5 mV. If the OCV of some cells is higher others, equalization is helpful to prolong the service life of the battery pack. Therefore, in

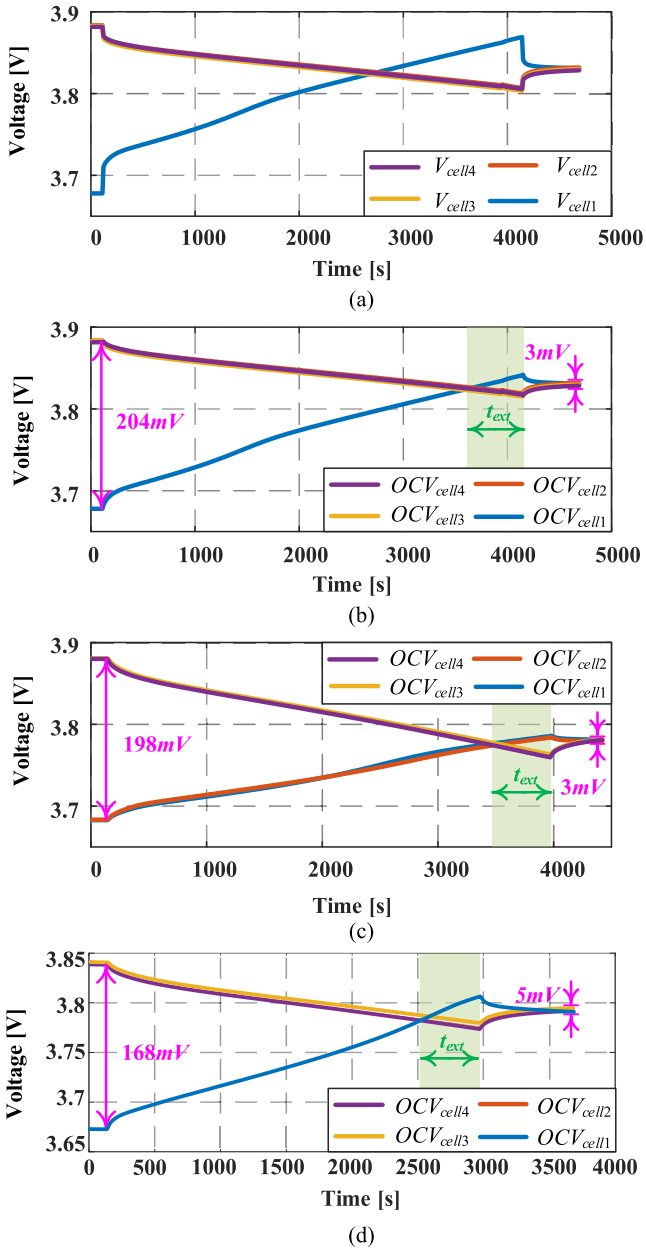

Fig. 15. Cell voltages during the equalization process with different balancing path. (a) The initial terminal voltages (V_{cell}) are 3.882, 3.882, 3.882, and 3.678 V. (b) The initial open-circuit voltages (OCV_{cell}). (c) The initial open-circuit voltages (V_{cell}) are 3.880, 3.880, 3.683, and 3.682 V. (d) The initial open-circuit voltages (V_{cell}) are 3.839, 3.841, 3.839, and 3.673 V.

discharging test [Fig. 17(b)], the initial voltages (OCV) are set to 3.832 V for strong cells, and 3.648 and 3.642 V for the weak cells. After 3900 s, the voltage difference decreases from 190 to 3 mV. As shown in Fig. 18, the calculated power losses of the proposed equalizer includes diode loss, transformer loss, inductor loss, MOSFET loss, and capacitor loss. The diode loss accounts for the main part of the total loss.

V. Comparison With Existing Battery Equalizers

In order to identify the advantages of the proposed equalizer, a comprehensive comparison is conducted. Tables II and III

TABLE II
COMPARISON OF DIFFERENT EQUALIZERS IN TERMS OF THE COMPONENT NUMBER

Topologies	MOSFETs & Drivers	SW stress	Diodes	Capacitors	Inductors	Transformer magnetic cores(windings)	Relays
Dissipative resistor [9]	N	V_c	0	0	0	0	0
Star-structure SCs [11]	$2N$	$\frac{V_c}{2}$	0	N-1	0	0	0
Transformer carrier [13]	$2N+6$	$\frac{V_c}{2}$	0	0	0	1(2)	0
Coupled half-bridge converter [14]	N	V_c	0	0	0	$\frac{N}{12}(\frac{N}{2})$	0
Flyback converter [15]	$2(N-1)$	NV_c	$2N-1$	0	0	1(2)	0
Quasi-resonant converter [16]	$2(N+1)+8$	NV_c	2	5	2	1(2)	0
Multi-stage inductor carrier [19]	$2N+6m$	$(N/m)V_c$	0	0	$m+1$	0	0
Multiport converter&Buck-Boost [20]	$2(N+m-1)$	$(N/m)Vc$	0	3m	$N-1$	$1(m)$	m
LLC & buck-boost [21]	$6m+2$	NV_c	2	2	3m	1(3)	$m+5$
Wave-trap equalizer [22]	2	NV_c	N	N	N	$N(2N)$	0
Half-bridge converter [26]	2	NV_c	$2N$	0	0	$\frac{N}{2}(\frac{3N}{2})$	0
This work	2	NV_c	2	2	1	1(3)	$2N$

The cell voltage is assumed equal to V_c. m and N is the number of cell modules and single cells,respectively.

TABLE III
COMPARISON OF DIFFERENT EQUALIZERS IN TERMS OF THE BALANCING PERFORMANCES

Topologies	Energy flow types	Frequency (kHz)	Open-loop current control	Constant speed	Current (A)	Efficiency (%)	Accuracy (%)
Dissipative resistor [9]	C2R	-	Y	N	-	0	-
Star-structure SCs [11]	C2C	28.57	Y	N	$1.02 \rightarrow 0$	93.1	-
Transformer carrier [13]	C2C	20	Y	Y	0.197	80.4	92
Coupled half-bridge converter [14]	C2C	10	Y	N	$1.2 \rightarrow 0$	95	-
Flyback converter [15]	C2S	25 & 37.5& 75	N	Y	0.15	$70 \sim 88$	89
Quasi-resonant converter [16]	C2S	20	N	Y	2 & 3	83.4	93
Multi-stage inductor carrier [19]	HME	40	Y	Y	0.223	88.4^m & 79.45	93
Multiport converter&Buck-Boost [20]	HME	100 & 120	N	Y	3.5 & 7.5	89.7	85
LLC & buck-boost [21]	HME	100 & (170∼230)	N	Y	1.5 (peak) & 1	86.74 & 89.66	95
Wave-trap equalizer [22]	S2C	$100 \sim 215$	N	Y	0.1	< 80	91
Half-bridge converter [26]	S2C	$100 \sim 200$	N	N	5 (peak)	93	75
This work	S2C	200	Y	Y	0.5	88.1	92

Y: Yes, N: No.
m is the stage number.

present a comparison of the proposed equalizer with existing solutions. The comparison focuses on main components count, voltage stress of MOSFETs, energy flow types, frequency, open-loop current control, constant speed, current, efficiency, and accuracy. The quantitative data such as frequency, current, efficiency, and accuracy are extracted from experimental results. The remaining qualitative parameters use binary criteria (Yes or No).

"Energy flow types" is determined by the available equalization paths and equalization structures. "Frequency" is the switching frequency, and higher frequency facilitates a more compact design. "Open-loop current control" is determined by the control algorithms, and whether the equalizer needs closed-loop control to adjust duty cycle and frequency. LLC and buck–boost solution in [21] achieve constant balancing current using frequency modulation, which leads to high control complexity. "Constant speed" is determined by whether the balancing current is constant. In [26], the balancing currents depend on the cell voltage difference. Therefore, the balancing speed degrades with the progress of balancing. The current mainly reflects the balancing speed. In constant speed equalizers, larger current can achieve faster balancing speed. "Efficiency" is measured by the conversion efficiency of equalizer circuit and the number of balancing cycles. If it is a multilevel-balancing structure, the overall efficiency is the product of the efficiency of all the layers. "Accuracy" is defined as the ratio between initial voltage difference and balanced voltage difference.

According to whether the equalization current decays or not, equalization methods are divided into constant current equalizations (CCEs) and non-constant current equalizations (NCCEs). Constant current output converter is a typical solution of CCE. Meanwhile, switched capacitor is one of the classical NCCEs. As shown in Fig. 19, the current in the NCCE decreases, because the equalization current is affected by the voltage difference

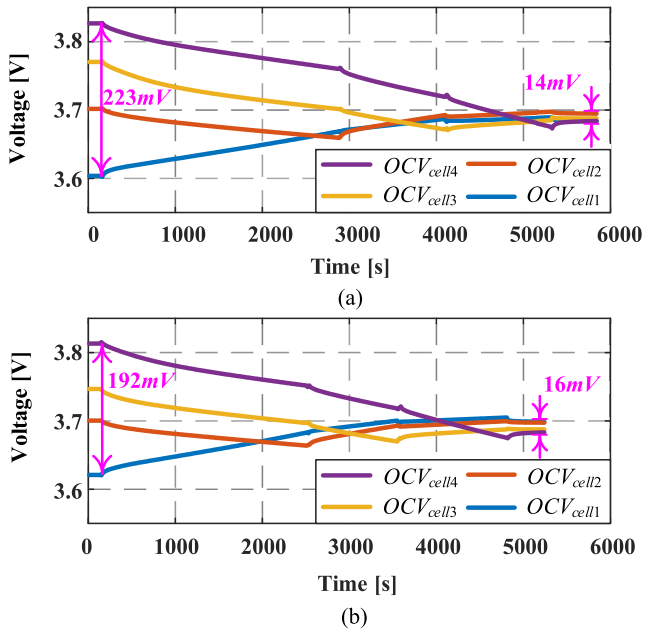

Fig. 16. Equalization results for four cells with different distributions. (a) Initial open-circuit voltages (OCV_{cell}) are 3.604, 3.702, 3.770, and 3.827 V. (b) Initial open-circuit voltages (OCV_{cell}) are 3.621, 3.701, 3.747, and 3.813 V.

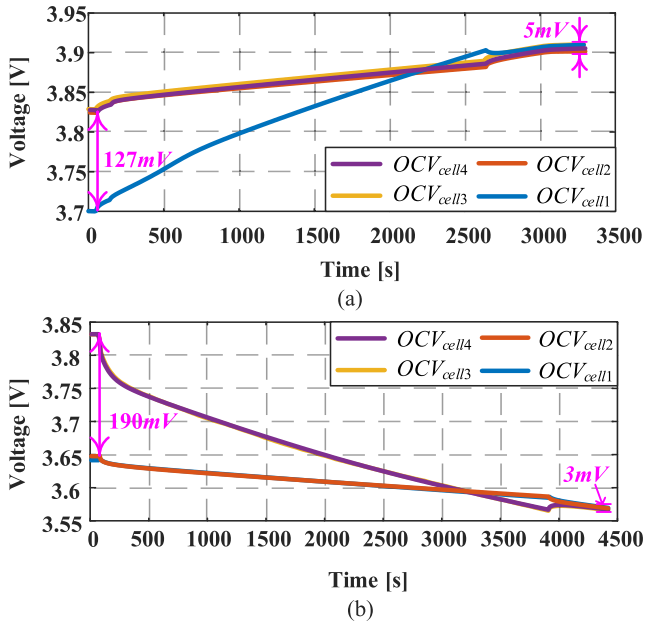

Fig. 17. Charging and discharging equalization results for four cells with different distributions. (a) Charging equalization and initial open-circuit voltage (OCV_{cell}) voltages are 3.828, 3.827, 3.824, and 3.701 V. (b) Discharging equalization and initial open-circuit voltage (OCV_{cell}) voltages are 3.832, 3.832, 3.648, and 3.642 V.

between the target cell and the source cell. Thus, the balancing speed gradually slowed down. In addition, the balancing time of CCEs (t_c) is significantly less than that of NCCEs (t_{nc}).

Active equalizers are also categorized into capacitor-based, inductor-based, and isolated converter-based. The isolated converters are widely used in C2S and S2C equalizers. Moreover, it

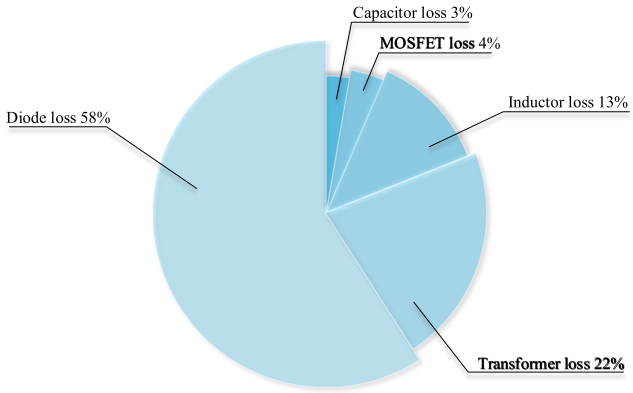

Fig. 18. Calculated power loss breakdown of design balancing circuit.

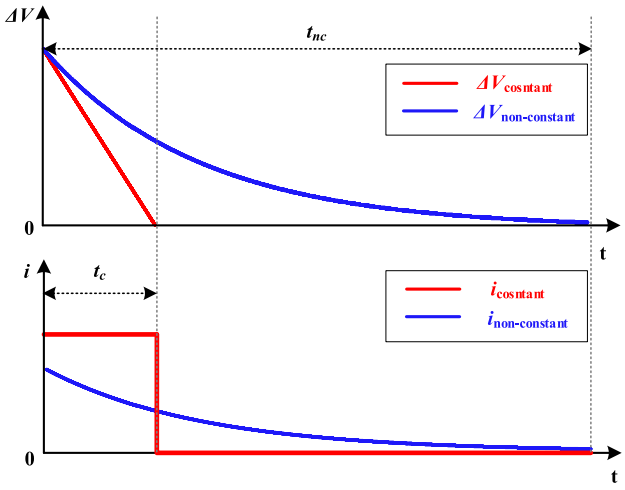

Fig. 19. Voltage difference and balancing current with two equalization methods.

can be used as the first stage of HME to improve balancing speed. In [36], a double-switch cell voltage equalizer using a parallel-resonant-inverter or series-parallel-resonant inverter and voltage multiplier is proposed for supercapacitors. This equalizer realizes constant current output with fixed switching frequency. However, due to the low efficiency, the attenuation of equalization current is very obvious. In [15], time-shared flyback converter-based equalizer is proposed, which utilizes a single converter to reduce size. However, only one balancing loop with 70% efficiency can operate at one moment. High energy loss leads to low balancing speed and thermal management problems. In [16], a quasi-resonant converter-based bidirectional C2S equalizer is proposed, where a two-winding transformer is shared via a multiplexer network. This design shows very good modularization, energy flow, and good balancing speed. The ZVS turn-ON of MOSFETs is realized by utilizing the quasi-resonant operation mode, which leads to improved efficiency. However, this requires additional components and complex control signals, leading to poor control complexity. In [21], hierarchical equalization architecture is based on half-bridge LLC resonant converter, and buck–boost converter is proposed. This structure utilizes hierarchical structure to improve energy-flow performance and introduces basic C2C to

facilitate the circuit extensibility. Unfortunately, double-layer structure requires complex control algorithm. Meanwhile, the switching frequency of LLC-based equalizer needs to be turned dynamically to ensure a constant balancing current, which also increases the control complexity.

It can be seen in Table II that LCC-based equalizer requires two MOSFETs and drivers. As with most converters, the voltage stress of MOSFETs depends on cells number. As shown in Table III, the switching frequency is high, which helps to reduce the volume. In addition, constant current facilitates simple estimation of battery state, which helps the controller make judgment on the equalization time. Open-loop control equalization balancing can reduce the control complexity effectively. Therefore, LCC-resonant converter is a good candidate for Li-ion battery equalizers.

In summary, the proposed equalizer exhibits good balancing accuracy. In addition, fewer components facilitate small size and weight. On the other hand, the equalizer achieves constant current balancing with constant f_s, which realizes low control complexity and easy implementation. Moreover, the balancing efficiency is good as all the MOSFETs and diodes can achieve ZVS turning ON and ZCS turning OFF, respectively. A high switching frequency can be selected. By designing circuit parameters properly, balancing current can be customized to realize the targeted balancing speed.

VI. Conclusion

In this article, a novel S2C battery equalizer with simplified constant current control is proposed based on fixed-frequency LCC resonant converter. The operation principle and key design considerations are explained in detail. The proposed equalizer utilizes the constant current characteristic of LCC-resonant circuit at its resonance frequency without auxiliary circuit. The proposed structure can achieve a direct path for charge transfer from the string to the single cell which minimizes the balancing cycles. In summary, the proposed system has the advantages of low cost, simple control, and easy implementation. A prototype to balance a four-cell battery string is designed and tested. The voltage difference after balancing is reduced by more than 92% compared with that before balancing. Both MOSFETs operate with ZVS and both diodes operate with ZCS, which enable a 200-kHz switching frequency. A peak conversion efficiency of 88.1% and overall good efficiency performance are recorded. Future work would investigate the impact of battery damage in the equalization system.

References

[1] Y. Li, J. Xu, X. Mei, and J. Wang, "A unitized multiwinding transformer-based equalization method for series-connected battery strings," *IEEE Trans. Power Electron.*, vol. 34, no. 12, pp. 11 981–11 989, Dec. 2019.

[2] D. F. Frost and D. A. Howey, "Completely decentralized active balancing battery management system," *IEEE Trans. Power Electron*., vol. 33, no. 1, pp. 729–738, Jun. 2018.

[3] C. Zhang, N. Cui, Z. Zhou, Y. Shang, B. Duan, and Q. Zhang, "Multi-cell-to-multi-cell equalizers based on matrix and half-bridge LC converters for series-connected battery strings," *IEEE J. Emerg. Sel. Top. Power Electron.*, vol. 8, no. 2, pp. 1755–1766, Jun. 2020.

[4] Y. Gao, C. Zhang, Y. Jiang, Q. Guo, J. Jiang, and W. Zhang, "Recognition of battery aging variations for $LiFePO_4$ batteries in 2nd use applications combining incremental capacity analysis and statistical approaches," *J. Power Sources*, vol. 360, pp. 180–188, 2017.

[5] J. Carter, Z. Fan, and J. Cao, "Cell equalisation circuits: A review," *J. Power Sources*, vol. 448, pp. 227–489, 2020.

[6] J. Gallardo-lozano, E. Romero-cadaval, M. I. Milanes-montero, and M. A. Guerrero-martinez, "Battery equalization active methods," *J. Power Sources*, vol. 246, pp. 934–949, 2014.

[7] L. Lu, X. Han, J. Li, J. Hua, and M. Ouyang, "A review on the key issues for lithium-ion battery management in electric vehicles," *J. Power Sources*, vol. 226, pp. 272–288, 2013.

[8] R. Guo, L. Lu, M. Ouyang, and X. Feng, "Mechanism of the entire overdischarge process and overdischarge-induced internal short circuit in lithium-ion batteries," *Sci. Rep.*, vol. 6, pp. 1–9, 2016.

[9] M. M. Hoque, M. A. Hannan, A. Mohamed, and A. Ayob, "Battery charge equalization controller in electric vehicle applications: A review," *Renewable Sustain. Energy Rev.*, vol. 75, pp. 1363–1385, 2017.

[10] T. H. Phung, A. Collet, and J.-C. Crebier, "An optimized topology for next-to-next balancing of series-connected lithium-ion cells," *IEEE Trans. Power Electron.*, vol. 29, no. 9, pp. 4603–4613, Sep. 2014.

[11] Y. Shang, N. Cui, B. Duan, and C. Zhang, "Analysis and optimization of star-structured switched-capacitor equalizers for series-connected battery strings," *IEEE Trans. Power Electron*., vol. 33, no. 11, pp. 9631–9646, Nov. 2018.

[12] M. Y. Kim, C. H. Kim, J. H. Kim, and G. W. Moon, "A chain structure of switched capacitor for improved cell balancing speed of lithium-ion batteries," *IEEE Trans. Ind. Electron.*, vol. 61, no. 8, pp. 3989–3999, Aug. 2014.

[13] K. M. Lee, S. W. Lee, Y. G. Choi, and B. Kang, "Active balancing of Li-ion battery cells using transformer as energy carrier," *IEEE Trans. Ind. Electron.*, vol. 64, no. 2, pp. 1251–1257, Feb. 2017.

[14] Y. Shang, N. Cui, and C. Zhang, "An optimized any-cell-to-any-cell equalizer based on coupled half-bridge converters for series-connected battery strings," *IEEE Trans. Power Electron.*, vol. 34, no. 9, pp. 8831–8841, Sep. 2019.

[15] A. M. Imtiaz and F. H. Khan, "Time shared flyback converter' based regenerative cell balancing technique for series connected Li-ion battery strings," *IEEE Trans. Power Electron*., vol. 28, no. 12, pp. 5960–5975, Dec. 2013.

[16] J. Lu, Y. Wang, and X. Li, "Isolated bidirectional dc–dc converter with quasi-resonant zero-voltage switching for battery charge equalization," *IEEE Trans. Power Electron.*, vol. 34, no. 5, pp. 4388–4406, May 2019.

[17] M. Einhorn, W. Roessler, and J. Fleig, "Improved performance of serially connected Li-ion batteries with active cell balancing in electric vehicles," *IEEE Trans. Veh. Technol.*, vol. 60, no. 6, pp. 2448–2457, Jul. 2011.

[18] C. S. Lim, K. J. Lee, N. J. Ku, D. S. Hyun, and R. Y. Kim, "A modularized equalization method based on magnetizing energy for a series-connected lithium-ion battery string," *IEEE Trans. Power Electron.*, vol. 29, no. 4, pp. 1791–1799, Apr. 2014.

[19] S. W. Lee, K. M. Lee, Y. G. Choi, and B. Kang, "Modularized design of active charge equalizer for Li-ion battery pack," *IEEE Trans. Ind. Electron.*, vol. 65, no. 11, pp. 8697–8706, Nov. 2018.

[20] Z. Zhang, H. Gui, D. J. Gu, Y. Yang, and X. Ren, "A hierarchical active balancing architecture for lithium-ion batteries," *IEEE Trans. Power Electron.*, vol. 32, no. 4, pp. 2757–2768, Apr. 2017.

[21] F. Peng, H. Wang, and Z. Wei, "An LLC-based highly efficient S2M and C2C hybrid hierarchical battery equalizer," *IEEE Trans. Power Electron.*, vol. 35, no. 6, pp. 5928–5937, Jun. 2020.

[22] M. Arias, J. Sebastián, M. M. Hernando, U. Viscarret, and I. Gil, "Practical application of the wave-trap concept in battery-cell equalizers," *IEEE Trans. Power Electron.*, vol. 30, no. 10, pp. 5616–5631, Oct. 2015.

[23] M. Uno and A. Kukita, "Two-switch voltage equalizer using an LLC resonant inverter and voltage multiplier for partially shaded series-connected photovoltaic modules," *IEEE Trans. Ind. Appl.*, vol. 51, no. 2, pp. 1587–1601, Mar./Apr. 2015.

[24] C. H. Kim, M. Y. Kim, H. S. Park, and G. W. Moon, "A modularized two-stage charge equalizer with cell selection switches for series-connected lithium-ion battery string in an HEV," *IEEE Trans. Power Electron.*, vol. 27, no. 8, pp. 3764–3774, Aug. 2012.

[25] M. A. Hannan *et al.*, "Lithium-ion battery charge equalization algorithm for electric vehicle applications," *IEEE Trans. Ind. Appl.*, vol. 53, no. 1, pp. 2541–2549, May/Jun. 2017.

[26] C. Hua and Y. Fang, "A charge equalizer with a combination of APWM and PFM control based on a modified half-bridge converter," *IEEE Trans. Power Electron.*, vol. 31, no. 4, pp. 2970–2979, Apr. 2016.
[27] F. Peng, H. Wang, and L. Yu, "Analysis and design considerations of efficiency enhanced hierarchical battery equalizer based on bipolar CCM buck–boost units," *IEEE Trans. Ind. Appl.*, vol. 55, no. 4, pp. 4053–4063, Jul./Aug. 2019.
[28] F. Baronti, R. Roncella, and R. Saletti, "Performance comparison of active balancing techniques for lithium-ion batteries," *J. Power Sources*, vol. 267, pp. 603–609, 2014.
[29] M. A. Hannan, M. M. Hoque, P. J. Ker, R. A. Begum, and A. Mohamed, "Charge equalization controller algorithm for series-connected lithium-ion battery storage systems: Modeling and applications," *Energies*, vol. 10, no. 9, 2017, Art no. 1390.
[30] R. L. Steigerwald, "A comparison of half-bridge resonant converter," *IEEE Trans. Power Electron.*, vol. 3, no. 2, pp. 174–182, Apr. 1988.
[31] A. J. Gilbert, D. A. Stone, C. M. Bingham, and M. P. Foster, "Design of an LCC current-output resonant converter for use as a constant current source," in *Proc. Eur. Conf. Power Electron. Appl.*, 2007, pp. 1–6.
[32] M. Chen and G. A. Rincon-Mora, "Accurate electrical battery model capable of predicting runtime and I-V performance," *IEEE Trans. Energy Convers.*, vol. 21, no. 2, pp. 504–511, Jun. 2006.
[33] A. Hentunen, T. Lehmuspelto, and J. Suomela, "Time-domain parameter extraction method for Thévenin-equivalent circuit battery models," *IEEE Trans. Energy Convers.*, vol. 29, no. 3, pp. 558–566, Sep. 2014.
[34] C. K. Chau, F. Qin, S. Sayed, M. H. Wahab, and Y. Yang, "Harnessing battery recovery effect in wireless sensor networks: Experiments and analysis," *IEEE J. Sel. Areas Commun.*, vol. 28, no. 7, pp. 1222–1232, Sep. 2010.
[35] *NCR18650PF Lithium Ion Cell Datasheet*, Panasonic, 2016. [Online]. Available: https://b2b-api.panasonic.eu/file_stream/pids/fileversion/3447
[36] M. Uno and A. Kukita, "Double-switch equalizer using parallel- or series-parallel-resonant inverter and voltage multiplier for series-connected supercapacitors," *IEEE Trans. Power Electron.*, vol. 29, no. 2, pp. 812–828, Feb. 2014.

Zhengqi Wei (Graduate Student Member, IEEE) received the B.S. degree in electronic information science and technology from Shaanxi Normal University (SNNU), Xi'an, China, in 2019. He is currently working toward the M.S. degree with the School of Information Science and Technology, ShanghaiTech University, Shanghai, China.

His research interests include battery management system and battery equalization.

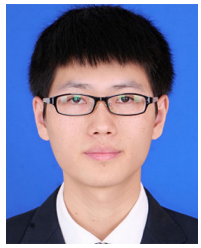

Faxiang Peng received the B.S. degree in electrical engineering and automation from the Xi'an University of Technology, Xi'an, China, in 2017, and the M.S. degree in microelectronics and solid-state electronics from the Chinese Academy of Sciences, Shanghai Institute of Microsystem and Information Technology, Shanghai, China, in 2020.

From 2017 to 2020, he was a Graduate Research Assistant with the Power Electronics and Renewable Energies Laboratory, School of Information Science and Technology, ShanghaiTech University, Shanghai, China. He is currently a Voltage Regulator Design Engineer with Data Platforms Group, Intel Asia-Pacific Research and Development Ltd., Shanghai, China, where he is involved with voltage regulator design of server in data center.

Mr. Peng was the Finalist of the IEEE IAS TSC Prize Paper Award in 2019 for his first-authored paper.

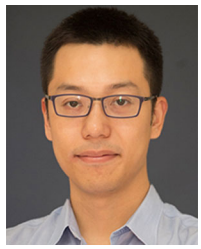

Haoyu Wang (Senior Member, IEEE) received the bachelor's degree (with distinguished hons.) in electrical engineering from Zhejiang University, Hangzhou, China, in 2009, and the Ph.D. degree in electrical engineering from the University of Maryland at College Park, College Park, MD, USA, in 2014.

In 2014, he joined the School of Information Science and Technology, ShanghaiTech University, Shanghai, China, where he is currently a tenured Associate Professor. His research interests include power electronics, plug-in electric and hybrid electric vehicles, the applications of wide-bandgap semiconductors, renewable energy harvesting, and power management integrated circuits.

Dr. Wang is an Associate Editor of the IEEE TRANSACTIONS ON INDUSTRIAL ELECTRONICS, the IEEE TRANSACTIONS ON TRANSPORTATION ELECTRIFICATION, and the *CPSS Transactions on Power Electronics and Applications.*